





# Optically induced antiferromagnetic order in dielectric metasurfaces with complex supercells

ASO RAHIMZADEGAN,<sup>1,\*</sup>  SERGEY LEPESHOV,<sup>2</sup>  WENJIA ZHOU,<sup>3,4</sup> DUK-YONG CHOI,<sup>5</sup>   
JÜRGEN SAUTTER,<sup>3</sup> DENNIS ARSLAN,<sup>3,4</sup> CHENGJUN ZOU,<sup>3,4</sup> STEFAN FASOLD,<sup>3</sup>  
CARSTEN ROCKSTUHL,<sup>1,6</sup> THOMAS PERTSCH,<sup>1,7</sup> YURI KIVSHAR,<sup>5</sup>  AND ISABELLE STAUE<sup>3,4</sup>

<sup>1</sup>*Institute of Theoretical Solid State Physics, Karlsruhe Institute of Technology, 76131 Karlsruhe, Germany*

<sup>2</sup>*ITMO University, St. Petersburg, Russia*

<sup>3</sup>*Institute of Applied Physics, Abbe Center of Photonics, Friedrich Schiller University Jena, 07745 Jena, Germany*

<sup>4</sup>*Institute of Solid State Physics, Friedrich Schiller University Jena, 07743 Jena, Germany*

<sup>5</sup>*Nonlinear Physics Center, Research School of Physics, Australian National University, Canberra, ACT 2601, Australia*

<sup>6</sup>*Institute of Nanotechnology, Karlsruhe Institute of Technology, 76021 Karlsruhe, Germany*

<sup>7</sup>*Fraunhofer Institute for Applied Optics and Precision Engineering, 07745 Jena, Germany*

\*aso.rahimzadegan@kit.edu

Metasurfaces are 2D planar lattices of nanoparticles that allow the manipulation of incident light properties. Because of that attribute, metasurfaces are promising candidates to replace bulky optical components. Traditionally, metasurfaces are made from a periodic arrangement of identical unit cells. However, more degrees of freedom are accessible if an increasing number of structured unit cells are combined. The present study explores a type of dielectric metasurface with complex supercells composed of Mie-resonant dielectric nanocylinders and nanoscale rings. We numerically and experimentally demonstrate the signature of an optical response that relies on the structures sustaining staggered optically induced magnetic dipole moments. The optical response is associated with an optical antiferromagnetism. The optical antiferromagnetism exploits the presence of pronounced coupling between dissimilar Mie-resonant dielectric nanoparticles. The coupling is manipulated by engineering the geometry and distance between the nanoparticles, which ultimately enhances their effective magnetic response. Our results suggest possible applications in resonant nanophotonics by broadening the modulation capabilities of metasurfaces.

## 1. INTRODUCTION

Metasurfaces have attracted a lot of attention in photonics in recent years [1–11]. Current trends call for creating highly transparent, functional, and active metasurfaces with high-index dielectric nanoparticles [12–14]. Dielectric nanoparticles with a high refractive index can be excited to sustain electric and magnetic Mie resonances at optical frequencies. The negligible absorption and strong scattering of dielectric resonant nanoparticles bring about a pronounced coupling of these components in a metasurface. As a result, the emergent electromagnetic response of a metasurface is vastly different from the response of the isolated nanoparticle [15,16]. The coupling effects in periodic metasurfaces with identical nanoparticles have been extensively studied [9,10,16–19]. However, coupling in periodic metasurfaces with dissimilar nanoparticles is less explored [15]. Note that coupling here refers to the renormalization of the optical response of the nanoparticles (for example, the resonance frequencies), when they interact with each other, as compared to their isolated optical responses.

Some years ago, it was predicted theoretically that a hybrid dimer structure composed of metal split-ring resonators and silicon nanospheres could exhibit a novel type of optically induced magnetic order termed as optical antiferromagnetic (AFM) order [20]. In the optical antiferromagnetic order, the induced magnetic dipole moments of the dissimilar nanoparticles are antiparallel. This is in contrast to the conventional parallel magnetic dipole (i.e., the optical ferromagnetic (FM) order), in which the induced dipole moments are equal and collinear. These effects have not been observed in optics. Still, theory predicted that a similar AFM order could be expected in anisotropic lattices composed of dielectric nanocylinders and nanotubes [21].

In this work, based on the theoretical work in [21], we have fabricated and analyzed all-dielectric periodic metasurfaces with complex supercells that, in contrast to unit cells containing only a single nanoparticle, give rise to what we believe, to the best of our knowledge, are novel scattering states, as shown in Fig. 1. The supercells of these metasurfaces are composed of

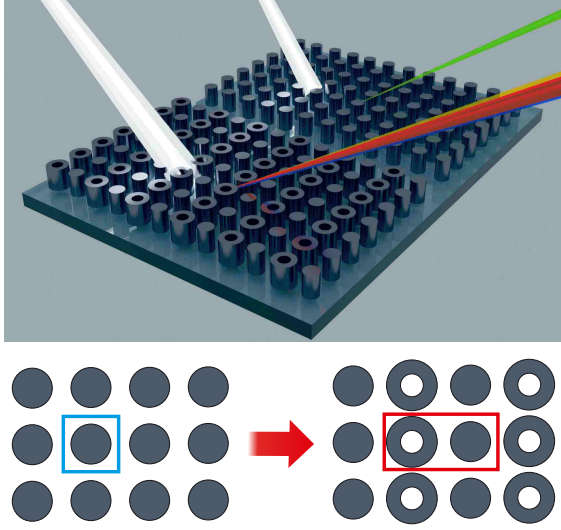


**Fig. 1.** A complex lattice unit cell: The transition from a single particle cell to a dimer cell gives rise to new scattering states.

two nanoparticles: a nanocylinder and a nanotube. These two dissimilar nanoparticles, in a complex supercell, have shown AFM order [21]. Here, we studied the optical response of metasurfaces with isotropic and anisotropic arrangements of these two components, as shown in Fig. 2 for a range of incidence angles, including normal incidence. The parameters are designed for the near-IR region. We experimentally demonstrated the signature of staggered magnetic dipole momenta in the transmittance spectra of the metasurfaces. We observed that AFM states can give rise to very high-quality resonances that extend over a wide range of incidence angles. The sharp resonance, like the Fano resonance or the bound state in the continuum, can be linked to the interference of the radiation from the antiparallel induced magnetic moments of dissimilar nanoparticles. By introducing dissimilar nanoparticles in the metasurface structure, new scattering states arise that provide more degrees of freedom to modulate the impinging light.

## 2. RESULTS AND DISCUSSION

### A. Metasurface Structure

We designed and fabricated two types of all-dielectric metasurfaces with complex unit cells composed of dissimilar nanoparticles of Mie-resonant nanocylinders and nanotubes. We should note that using two nanocylinders with different sizes can also lead to AFM states. However, the nanotube can provide a broader magnetic resonance, which facilitates the design process. In the design process, we have looked for setups with pronounced antiparallel magnetic moments. Figure 2(a) shows the structure and scanning electron micrograph of an anisotropic metasurface composed of periodic rows of nanocylinders and nanotubes termed an “anisotropic metasurface.” Figure 2(b) shows the “isotropic metasurface” composed of a checkerboard lattice of nanotubes and nanocylinders. The size parameters are mentioned in the figure caption. The design follows our theoretical study in [21].

The materials used for the nanoparticles and the substrate are silicon and silica glass, respectively. For wavelengths between

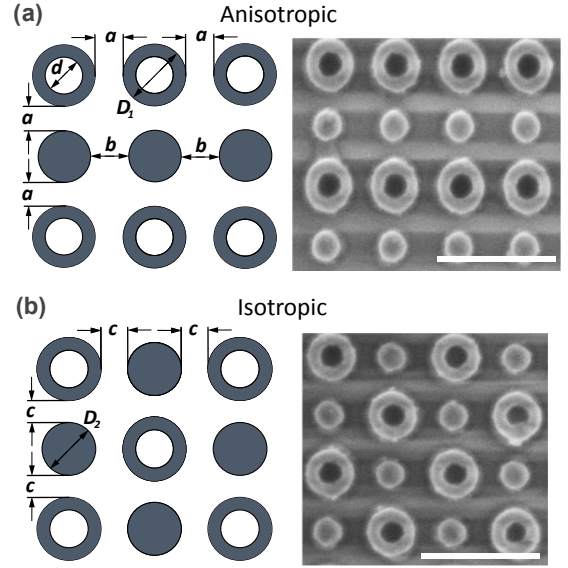


**Fig. 2.** Two types of silicon metasurfaces with a complex unit cell composed of dissimilar periodic lattices of resonant nanocylinders and nanotubes: (a) Structure and scanning electron micrograph of a metasurface composed of periodic rows of nanocylinders and nanotubes, termed an anisotropic metasurface. Here,  $a = 150$  nm and  $b = 300$  nm. The periodicity of the supercell is 930 nm and 550 nm. (b) The isotropic metasurface is composed of a checkerboard lattice of nanoparticles. Here,  $c = 185$  nm. For both arrangements, the nanotube outer diameter is  $D_1 = 400$  nm, the nanotube inner diameter is  $d = 200$  nm, and the nanocylinder diameter is  $D_2 = 230$  nm. The periodicity of the supercell is  $500\sqrt{2} \approx 707$  nm. Each nanoparticle has a height of 300 nm. The scale bars are 1  $\mu$ m.

950 and 1600 nm, the two materials have a small dispersion. Furthermore, the absorption losses are negligible. In this wavelength range, the refractive index of silicon and silica is about 3.5 and 1.5, respectively. The silicon nanoparticles, nanocylinders, and nanotubes are fabricated on a thick glass substrate with the surrounding material being air.

### B. Methods

To fabricate the metasurface, we coated a 300 nm thick hydrogenated amorphous silicon (a-Si:H) film onto glass (SCHOTT-N-BK7, Schott AG) via plasma-enhanced chemical vapor deposition (PECVD). First, a positive electron beam resist (ZEP520A, Zeon Corp.) was spin-coated on the film. In the next step, the nanoparticle patterns were formed using e-beam lithography and the subsequent development in ZED-N50 (Zeon). Next, a 50 nm thick aluminum layer was evaporated onto the sample. Then, the resist was removed using ZDMAC (Zeon). The silicon film was etched in  $\text{CHF}_3$  plasma with a small addition of  $\text{SF}_6$ , which led to a highly anisotropic etching profile. Finally, the residual aluminum etch mask was removed using a wet etching solution.

To measure the metasurface transmittance spectra, we used an automated custom-built incoherent white light spectroscopy setup with complete control over the incidence angle and polarization. The sample was mounted on an automated step motor to not only move the sample, but also to rotate it along a single axis for the angular measurements. The setup had an

NA of 0.044, which corresponds to a half-angle of  $2.5^\circ$ . The divergence angle (half-angle) of the incident beam equaled  $0.8^\circ$ . The spectrometer used a scanning slit that corresponds to a 2 nm bandwidth, but the scanning was done in 0.8 nm steps. Moreover, the angular spectrum was sampled in steps of  $2^\circ$ .

We used a finite element method (using CST Studio Suite) to simulate the transmittance of the metasurfaces and the induced magnetic field distribution of the nanoparticles inside the lattice.

### C. Transmittance for Normal Incidence

In this subsection, we focus on the anisotropic metasurface under normal incidence illumination. Figures 3(a) and 3(b) show the simulated transmittance spectra calculated under normal incidence for the all-dielectric metasurface with an anisotropic arrangement of nanocylinders and nanotubes, as shown in Fig. 2(a). The insets show the magnetic field distribution in designated resonance frequencies. The transmittance spectra are very different for the two polarizations of the external field, and they reflect different types of resonances supported by the metasurfaces.

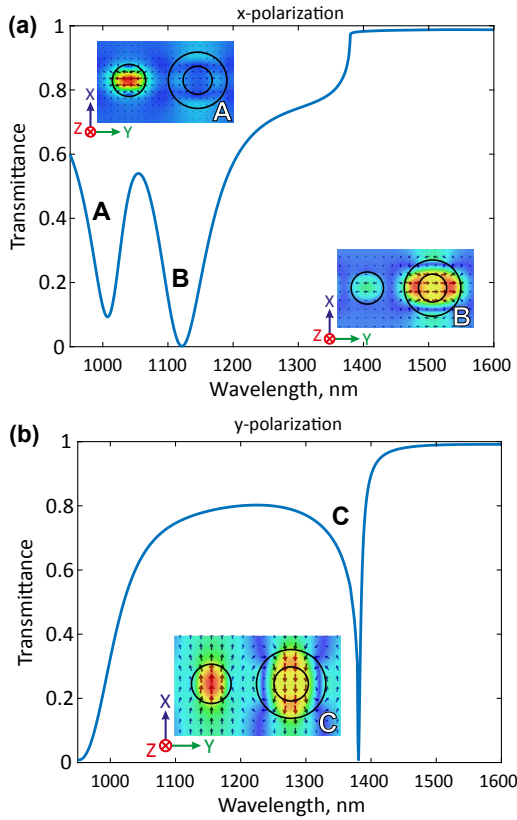


**Fig. 3.** Transmittance spectra of all-dielectric metasurfaces with anisotropic arrangements of nanocylinders and nanotubes as shown in Fig. 2(a), for two different polarizations of the external field: (a)  $x$ -polarization, and (b)  $y$ -polarization. For  $x$ -polarization, two distinct magnetic dipole resonances are observed at 1010 nm and 1124 nm (mode A and mode B), as shown in the insets of (a). For  $y$ -polarization, a hybrid response with the AFM order is observed at 1397 nm (mode C), as confirmed by the magnetic field distribution shown in the inset. The onset of the first diffraction order is at  $930 \text{ nm} \times 1.5 = 1395 \text{ nm}$ .

For  $x$  polarization [Fig. 3(a)] (i.e., a magnetic field along the  $y$  axis), two distinct magnetic dipole resonances are observed at wavelengths of 1010 nm and 1124 nm (mode A and mode B), as shown in the insets of Fig. 3(a). For mode A, the magnetic dipole moment of the nanocylinder is dominant with an out-of-phase resonance; for mode B, the magnetic dipole of the nanotube is dominant with an in-phase resonance. The sudden transition at 1400 nm is due to the onset of the first diffraction order.

For  $y$  polarization, as shown in Fig. 3(b), at the resonance mode C, a hybrid resonance with an AFM order is observed at 1397 nm. The magnetic field distribution, shown in the inset, displays an antiparallel orientation of the induced magnetic dipole moments of the nanotube and the nanocylinder. It is observed that the induced magnetic dipole moment of the nanotube is in-phase with the external magnetic field, while the induced dipole moment of the nanocylinder is out-of-phase. The pronounced coupling of the two nanoparticles led to the emergence of a what we believe is a novel antiparallel mode. A strong magnetic interaction near the onset of diffraction has also been observed in the literature [22]. We noticed that such an antiparallel mode cannot exist for periodic arrangements with unit cells composed of single nanoparticles.

As explained in [21], AFM and FM states can be tuned by changing the distances of nanotubes and nanocylinders. With an increasing distance, the coupling of the nanocylinders and nanotubes decays rapidly and the AFM modes cannot be excited. At a closer distance, the AFM-like response can be excited with an induced magnetic moment and opposite phase among dissimilar nanoparticles. The distance-dependent magnetic response is a unique feature of a complex supercell structure. The sensitivity of the AFM mode to slight variations manifests in the observed high-quality resonance. Due to this sensitivity, however, the mode is prone to fabrication defects, which makes experimental observations challenging.

### D. Metasurface Characterization

This subsection shows the experimental characterization of the fabricated metasurfaces for an extended illumination angle of up to  $30^\circ$ , and the results are compared to the simulation data.

Figure 4 shows the simulated and experimental data for the transmittance of the anisotropic and isotropic metasurfaces under oblique TE- and TM-polarized light illuminated in the  $XZ$  or  $YZ$  plane. The axes are shown in the inset. The simulation and experimental measurements show good agreement, especially for pronounced resonances.

The complex structure of the supercell leads to the splitting of the fundamental magnetic dipole mode of a single nanoparticle into various modes with different polarization and order of the dipoles. The transmittance dips observed in the experimental measurement is the evident fingerprints of the AFM/FM ordering predicted by the simulations. From the calculation of the magnetic field distributions of the modes at the resonances obtained using CST, we derived two types of modes: AFM magnetic modes with  $x$ ,  $y$ , and  $z$  orientation of the moments and FM magnetic modes directed along the  $y$  axis. We have marked these modes in Fig. 4 with black dashed lines. Remarkably, the FM order occurs only along the  $y$  axis [Figs. 4(b) and 4(e)] when the magnetic field vector is parallel to the dimer axis.

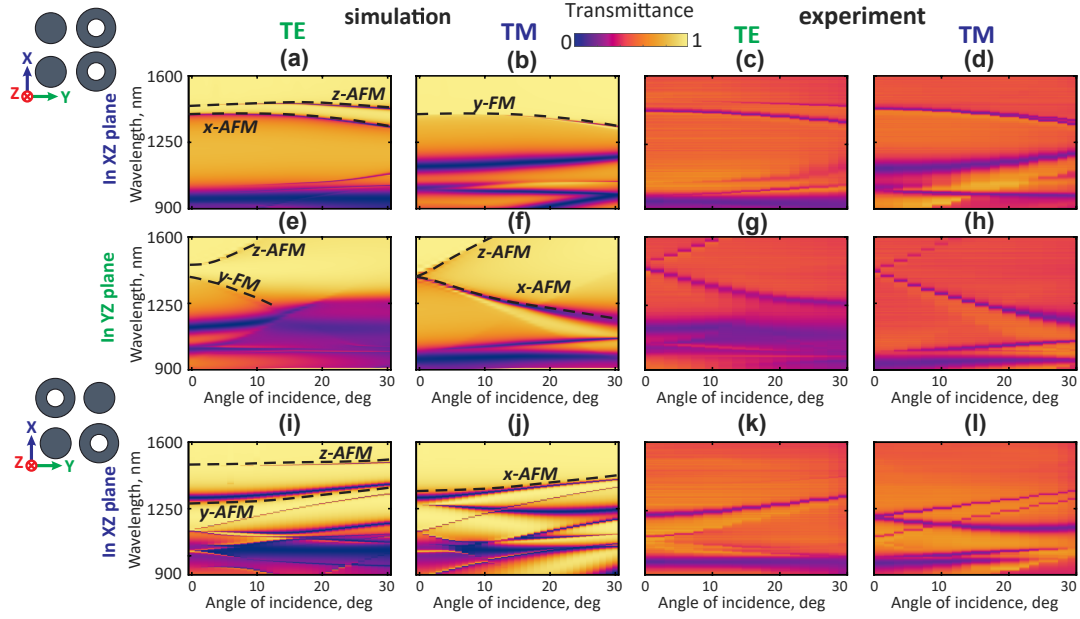


**Fig. 4.** (a)–(d) Experimental and simulated spectral and angular dependence of transmittance of anisotropic metasurface for TE- and TM-polarized light incident in the YZ plane. (e)–(h) Same dependence of transmittance for light incident in the XZ plane. (i)–(l) Experimental and simulated spectral and angular dependence of transmittance of isotropic metasurface for TE- and TM-polarized light incident in the XZ plane. The black dashed lines highlight the FM and AFM modes of the proposed metasurfaces.

Note that Figs. 4(b) and 4(e) are equivalent for normal incidence. Their transmittance spectrum is plotted in Fig. 3(a) (titled as the  $x$  polarization). Moreover, Figs. 4(a) and 4(f) are also equivalent for normal incidence angles. Their transmittance spectrum is plotted in Fig. 3(b) (titled as the  $y$  polarization). The C mode in Fig. 3(b) is an  $x$ -AFM mode, as the antiparallel dipole moments are in the  $x$  axis.

A deviation from the normal incidence opens the scattering channel for modes with a  $z$  axis oriented AFM state [cf. Figs. 4(a), 4(e), 4(f), and 4(i)]. At normal incidence, the magnetic field vector is directed along the  $x$  or  $y$  axis. Therefore, it prevents the coupling of the incident wave to the vertically polarized magnetic AFM mode. However, an external magnetic field along the  $z$  axis enables an antiparallel magnetic dipole moment excitation along the  $z$  axis. Interestingly, this mode can already appear for a very slight deviation from normal incidence.

Compared to the simulated data note that the experimental measurements for the transmittance were substantially lower, and the dips were substantially less pronounced. These discrepancies are due to fabrication imperfections. As evident from the SEM images of Fig. 2, the surfaces were not as smooth as assumed in the simulations. This roughness caused the light to scatter into a nonspecular, diffusive direction that is not collected by the spectrometer. Moreover, contamination of the sample would have a similar effect. In addition, the size of the nanoparticles was not as homogeneously distributed as designed; this undesired disorder can lead to the broadening and dampening of resonances. Finally, the actual material from which the resonators were made could also suffer from a higher density of surface states. These, indeed, could lead to an additional absorption that affects the background transmission over an extended spectral region.

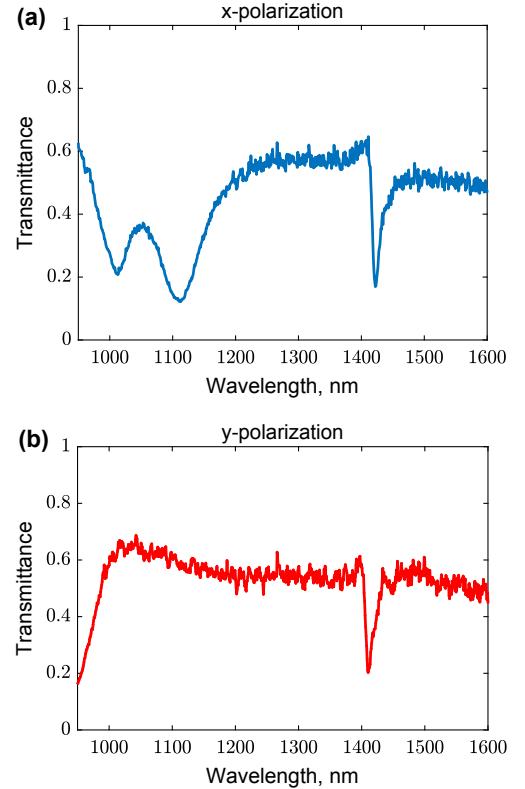


**Fig. 5.** Experimental transmittance spectra of the anisotropic metasurface measured for (a)  $x$ -polarized and (b)  $y$ -polarized plane waves.

Figure 5 shows the measured spectra for the anisotropic metasurface under normal incidence. The results can be compared to the simulated data in Fig. 2. Moreover, the data shall



be interpreted with a look at the experimental angular data of Fig. 4.

For  $x$  polarization [Fig. 5(a)], as predicted in the simulation results [Fig. 3(a)], two distinct magnetic dipole resonances were observed at wavelengths near 1000 and 1100 nm. Furthermore, we also observed a resonance at around 1400 nm. This resonance was not predicted in the simulation results. However, comparing the experimental and simulation results in Figs. 4(b) and 4(d) for tilted angles, we observed a resonance ( $y$ -FM) that has been broadened in the experimental results. Therefore, we ascribed this dip to a slight angular misalignment in the measurement setup and also broadening of resonances due to imperfections that have resulted in the resonance around 1400 nm.

For a  $y$  polarization incidence [Fig. 5(b)], a resonance was observed near 1400 nm. As predicted by the simulations, this resonance could be linked to the  $y$ -AFM mode. However, the resonance was not as sharp as in the simulations. Fabrication imperfections can explain the broadening and reduction in sharpness. Lattice constants can be quite precise during fabrication, while nanoparticle sizes can be prone to imperfections in the fabrication.

### 3. CONCLUSION

We studied Mie-resonant dielectric metasurfaces with a complex supercell created by two types of resonant dielectric nanoparticles (namely, nanocylinders and nanotubes) arranged in square/rectangular lattices. We demonstrated, for the first time to the best of our knowledge, the effects of pronounced near-field coupling of meta-atoms in such dielectric metasurfaces that can be observed in the optically induced staggered magnetic dipole moments. We revealed that the overall optical response of the metasurfaces depends on the mode hybridization and nanoparticle ordering. In particular, we observed an optically induced response corresponding to a staggered structure of optically induced magnetic dipole moments that can be associated with the physics of the so-called artificial optical antiferromagnetism. We believe our results may suggest novel applications in resonant nanophotonics by broadening the modulation capabilities of metasurfaces with complex unit cells.

**Funding.** Alexander von Humboldt-Stiftung; Australian Research Council (DP210101292); Deutsche Forschungsgemeinschaft (RO 3640/7-2, 1524/10-2, STA 1426/1-2 (278747906), STA 1426/2-1, the Excellence Cluster 3D Matter Made to Order (EXC 2082/1 (390761711)), CRC 1375 (398816777)); Army Research Office (FA520921P0034).

**Acknowledgment.** Author Yuri Kivshar acknowledges Boris Lukyanchuk for encouraging discussions of the problem at the initial stage of this project. Kivshar acknowledges financial support from the Australian Research Council, International Technology Center Indo-Pacific (ITC IPAC) via the Army Research Office, and the Alexander von Humboldt Foundation. Credits: Author Aso Rahimzadegan did the writing, editing, experimental measurement, and setup. Author Sergey Lepeshov did the simulations and plotted the figures. Author Wenjia Zhou contributed to the writing, simulations, and measurements. Author Duk-Yong Choi fabricated the samples. Author Dennis Arslan built the experimental measurement setup and contributed to the writing. Author Chengjun Zou contributed to the analysis of the modes. Author Stefan Fasold measured the SEM images. Author Jürgen Sautter supervised

the project. Finally, authors Kivshar, Carsten Rockstuhl, Isabelle Staude, and Thomas Pertsch reviewed and edited the paper and supervised the project.

**Disclosures.** The authors declare no conflicts of interest.

**Data availability.** Data underlying the results presented in this paper are not publicly available at this time, but may be obtained from the authors upon reasonable request.

### REFERENCES

1. N. Yu and F. Capasso, "Flat optics with designer metasurfaces," *Nat. Mater.* **13**, 139–150 (2014).
2. S. Chen, W. Liu, Z. Li, H. Cheng, and J. Tian, "Metasurface-empowered optical multiplexing and multifunction," *Adv. Mater.* **32**, 1805912 (2019).
3. O. Quevedo-Teruel, H. Chen, A. Diaz-Rubio, *et al.*, "Roadmap on metasurfaces," *J. Opt.* **21**, 073002 (2019).
4. H.-T. Chen, A. J. Taylor, and N. Yu, "A review of metasurfaces: physics and applications," *Rep. Prog. Phys.* **79**, 076401 (2016).
5. Y. Bao, J. Ni, and C.-W. Qiu, "A minimalist single-layer metasurface for arbitrary and full control of vector vortex beams," *Adv. Mater.* **32**, 1905659 (2019).
6. A. Rahimzadegan, D. Arslan, D. Dams, A. Groner, X. Garcia-Santiago, R. Alaee, I. Fernandez-Corbaton, T. Pertsch, I. Staude, and C. Rockstuhl, "Beyond dipolar Huygens' metasurfaces for full-phase coverage and unity transmittance," *Nanophotonics* **9**, 75–82 (2019).
7. X. Ni, A. V. Kildishev, and V. M. Shalaev, "Metasurface holograms for visible light," *Nat. Commun.* **4**, 2807 (2013).
8. L. Huang, S. Zhang, and T. Zentgraf, "Metasurface holography: from fundamentals to applications," *Nanophotonics* **7**, 1169–1190 (2018).
9. V. E. Babicheva and A. B. Evlyukhin, "Metasurfaces with electric quadrupole and magnetic dipole resonant coupling," *ACS Photon.* **5**, 2022–2033 (2018).
10. A. Rahimzadegan, T. D. Karamanos, R. Alaee, A. G. Lamprianidis, D. Beutel, R. W. Boyd, and C. Rockstuhl, "A comprehensive multipolar theory for periodic metasurfaces," *Adv. Opt. Mater.* **10**, 2102059 (2022).
11. C.-W. Qiu, T. Zhang, G. Hu, and Y. Kivshar, "Quo vadis, metasurfaces?" *Nano Lett.* **21**, 5461–5474 (2021).
12. S. Kruk and Y. Kivshar, "Functional meta-optics and nanophotonics governed by Mie resonances," *ACS Photon.* **4**, 2638–2649 (2017).
13. I. Staude, T. Pertsch, and Y. S. Kivshar, "All-dielectric resonant meta-optics lightens up," *ACS Photon.* **6**, 802–814 (2019).
14. J. Hu, A. I. Kuznetsov, V. J. Sorger, and I. Staude, "Tunable nanophotonics," *Nanophotonics* **11**, 3741–3743 (2022).
15. N. Liu and H. Giessen, "Coupling effects in optical metamaterials," *Angew. Chem. – Int. Ed.* **49**, 9838–9852 (2010).
16. S. Tretyakov, *Analytical Modeling in Applied Electromagnetics* (Artech House, 2003).
17. A. Epstein and G. V. Eleftheriades, "Huygens' metasurfaces via the equivalence principle: design and applications," *J. Opt. Soc. Am. B* **33**, A31–A50 (2016).
18. A. B. Evlyukhin, V. R. Tuz, V. S. Volkov, and B. N. Chichkov, "Bianisotropy for light trapping in all-dielectric metasurfaces," *Phys. Rev. B* **101**, 205415 (2020).
19. M. B. Ross, C. A. Mirkin, and G. C. Schatz, "Optical properties of one-, two-, and three-dimensional arrays of plasmonic nanostructures," *J. Phys. Chem. C* **120**, 816–830 (2016).
20. A. E. Miroshnichenko, B. Luk'yanchuk, S. A. Maier, and Y. S. Kivshar, "Optically induced interaction of magnetic moments in hybrid metamaterials," *ACS Nano* **6**, 837–842 (2012).
21. S. Lepeshov and Y. Kivshar, "Near-field coupling effects in Mie-resonant photonic structures and all-dielectric metasurfaces," *ACS Photon.* **5**, 2888–2894 (2018).
22. A. Rahimzadegan, R. Alaee, T. D. Karamanos, R. W. Boyd, and C. Rockstuhl, "Colossal enhancement of the magnetic dipole moment by exploiting lattice coupling in metasurfaces," *J. Opt. Soc. Am. B* **38**, C217–C224 (2021).